LA-UR-01-6968
Approved for public release; distribution is unlimited.

Title: **Magnetic Resonance Force Microscopy and the Solid State Quantum Computer**

Author(s): D.V. Pelekhov, I. Martin, A. Suter., D.W. Reagor, and P.C. Hammel

Submitted to:

http://lib-www.lanl.gov/cgi-bin/getfile?00796978.pdf

Magnetic Resonance Force Microscopy and the Solid State Quantum Computer

D.V. Pelekhov, I. Martin, A. Suter*, D.W. Reagor, and P.C. Hammel
Los Alamos National Laboratory, Los Alamos NM 87545
(January 11, 2002)

A Quantum Computer (QC) is a device that utilizes the principles of Quantum Mechanics to perform computations. Such a machine would be capable of accomplishing tasks not achievable by means of any conventional digital computer, for instance factoring large numbers. Currently it appears that the QC architecture based on an array of spin quantum bits (qubits) embedded in a solid-state matrix is one of the most promising approaches to fabrication of a scalable QC. However, the fabrication and operation of a Solid State Quantum Computer (SSQC) presents very formidable challenges; primary amongst these are: (1) the characterization and control of the fabrication process of the device during its construction and (2) the readout of the computational result. Magnetic Resonance Force Microscopy (MRFM)—a novel scanning probe technique based on mechanical detection of magnetic resonance–provides an attractive means of addressing these requirements. The sensitivity of the MRFM significantly exceeds that of conventional magnetic resonance measurement methods, and it has the potential for single electron spin detection. Moreover, the MRFM is capable of true 3D subsurface imaging. These features will make MRFM an invaluable tool for the implementation of a spin-based QC. Here we present the general principles of MRFM operation, the current status of its development and indicate future directions for its improvement.

I. INTRODUCTION

The last several decades have seen outstanding progress in development of conventional digital computing. A remarkable increase in processing power has been accompanied by parallel reduction in the size of the transistors used in contemporary processors. However, in spite of these advancements, there are significant tasks that cannot be easily performed due to the inherent binary/linear method of calculations used in contemporary computers; an example is factoring large numbers. This is a problem of great interest for information security and cryptography. For instance, it would take the fastest existing supercomputer billions of years to factor a 400 digit number [1], thus rendering any encryption code based factoring large numbers "unbreakable". Another problem that cannot be successfully solved by a conventional computer is modeling large quantum-mechanical systems. This problem is extremely interesting from the scientific point of view for understanding the fundamental principles of nature which in turn will lead to the development of materials with new properties and functionalities. Because the number of variables needed to describe a quantum mechanical system grows exponentially with its size, the ability to model large quantum mechanical systems using conventional computers is very limited.

Fortunately, there is an approach alternative to the binary computational mechanism employed in the existing computers. This method utilizes the principles of quantum mechanics to perform computations. A computing device based on such a method is called a Quantum Computer (QC). In such a computer, conventional bits are replaced with two level quantum systems, so-called quantum bits or qubits. Unlike a conventional bit, which can only assume one of its base values 0 and 1 at a time, a two level qubit with base states $|0\rangle$ and $|1\rangle$ can exist in a superposition of these base states with two complex coefficients describing the relative probability and phase of each of the base states. Thus, in order to describe an N qubit quantum system, one would need 2^N parameters (compared to N parameters in the case of a classical system). This intrinsic feature of a quantum computer allows performance of massively parallel computations on a single computer. A QC opens new avenues in information processing unavailable to conventional computers. However, exploiting this massive parallelism is a significant challenge, and this approach does not lend itself to application to arbitrary computational problems. The invention by P.W. Shor [2,3] of an algorithm for factoring large numbers using a quantum computer was an important breakthrough that demonstrated the importance of the QC for the future of information processing. He demonstrated that with such a machine this task can be completed within a manageable time thus potentially making it possible to decode otherwise "unbreakable" codes. There have also been very promising developments in the field of modeling quantum mechanical systems. Recently, G. Ortiz *et al.,* demonstrated an approach to simulation of fermionic systems on a quantum computer [4].

However, a practical quantum computer has yet to be developed. There are several major difficulties to

be overcome in order to build a QC. An issue of central importance is that of decoherence in quantum systems. The delicate phase relationships between the qubits existing in quantum superpositional states must be maintained over the time span required to complete a computation in order for it to function; to achieve this the qubits must be effectively isolated from the environment of the computer. Uncontrolled external influence will cause the superposition to decohere leading to collapse of the states, thus rendering computation impossible. Because of the fragility of these states, decoherence imposes a strong constraint on the development of a QC. Nevertheless several approaches to quantum computation that incorporate acceptably slow decoherence processes have been proposed, and there have been notable successes in demonstrating the quantum manipulations that will be essential for a quantum computer using, *e.g.,* trapped ions [5,6]. However, to be useful for problems such as factorization, a quantum computer design must be intrinsically scalable up to very large numbers of qubits; solid state implementations are very attractive from this point of view.

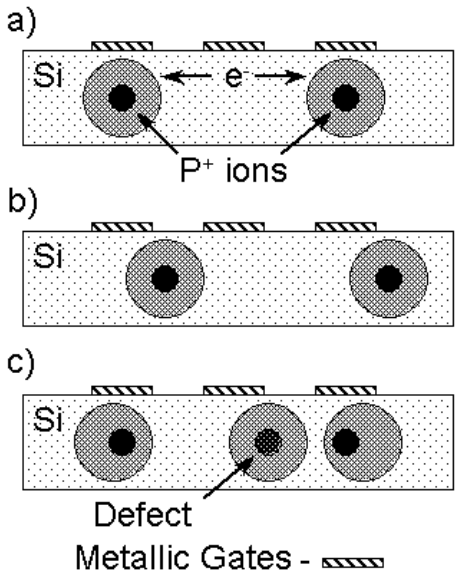

FIG. 1. Schematic diagram of the Solid State Quantum Computer [7]. a) A buried array of qubits (phosphorus atoms) with registered metallic control gates. Potential problems in a fabricated device might include b) misaligned gates, and c) unintentional defects.

A very promising design for a scalable quantum computer was proposed by B.E. Kane in 1998 [7]. This design is based on using the nuclear spins of phosphorus atoms embedded in a silicon matrix as the qubits whose states are defined by the two quantum states of the nuclear spin. As shown in Fig. 1, these atoms will be fabricated with atomic precision into an array buried at a depth of approximately 100–200 Å beneath the surface and with a well-controlled separation of approximately 200 Å between the atoms. Interactions between the qubits will be mediated by the electrons bound to the phosphorus atoms at the low temperatures at which the computer will operate. A second essential feature of the architecture is placement of control gates on the surface of the silicon; their location must be precisely registered to the underlying phosphorus qubit array. Controlled electrostatic potentials on metallic control gates will enable control of single and multi-qubit operations when applied in conjunction with conventional NMR techniques (Fig. 1a).

Clearly, fabrication of such a device is an extremely challenging task. The atoms must be precisely located in an ordered array with a pattern of metallic gates indexed relative to the array with atomic-scale precision. Any error in this process will result in gate misalignment (Fig. 1b). The SSQC will be fabricated out of ultra pure materials with a low density of defects, since any unwanted perturbation, such as an extra phosphorus atom or defects in the silicon crystal lattice (Fig. 1c) in the vicinity of a qubit can render the device useless for quantum computation. This makes clear that successful fabrication of a solid state quantum computer (SSQC) will require a characterization instrument that is capable of very high resolution subsurface imaging of both qubits and defects.

Once the SSQC has been created the process of its operation is equally challenging. One of the challenges is the readout of the result of a calculation. Although the quantum calculation is performed on a nuclear spin of a phosphorus atom, as a consequence of the hyperfine interaction between the nuclear spin and the bound electron, the result of the calculation can be read out via detection of a spin state of the bound electron. Read-out mechanisms exploiting the coupling between the spin and orbital wavefunction of the electronic have led to proposals for electron spin readout using single electron devices [7,8], however, it will be essential to have direct spin probes to complement these charge based techniques.

II. MAGNETIC RESONANCE FORCE MICROSCOPY AS A TOOL FOR QUANTUM COMPUTING

The drive to improve the sensitivity of magnetic resonance measurements have led to a variety of inventive

approaches. All of them involve development of detection techniques alternative to the conventional inductive method, including optical [9–11] and SQUID detection [12]. Another approach has been proposed by J.A. Sidles [13,14] who introduced the concept of the Magnetic Resonance Force Microscope (MRFM). This is a novel scanning probe method based on mechanical detection of magnetic resonance. This method is much more sensitive than the conventional methods of detection. It appears that its ultimate limit is detection of the signal from a single electron spin. The MRFM is a hybrid of the Atomic Force Microscope (AFM) and Magnetic Resonance Imaging (MRI) and thus is capable of fully three dimensional (3D) subsurface imaging [15,14]. Its potential single electron spin sensitivity combined with the subsurface imaging capability makes MRFM exceptionally well situated to provide both characterization of the QC during its fabrication and serve as a readout mechanism during its operation.

III. MAGNETIC RESONANCE FORCE MICROSCOPY: GENERAL PRINCIPLES

The method is based on coupling of a sample magnetic moment $\boldsymbol{m}$ to a probe magnet via the force of magnetic interaction:

$$\boldsymbol{F}(\boldsymbol{x},t) = -[\boldsymbol{m}(\boldsymbol{x},t)\cdot\boldsymbol{\nabla}]\boldsymbol{B}_{\rm probe}(\boldsymbol{x}) \qquad (1)$$

The strength of this interaction is proportional to the gradient of the inhomogeneous magnetic field of the probe magnet, which can be made very high. This force of interaction is measured through detection of the displacement of a compliant micro-mechanical resonator that is deflected by the applied force. The sensitivity of this approach is ultimately limited by the thermomechanical noise of the resonator. If the magnetic moments under study are manipulated at the resonant frequency of the mechanical resonator, its displacement is magnified by the quality factor Q of the resonator, which can be as high as 10^5, compared to the displacement resulting from a DC force of the same magnitude. The combination of high magnetic field gradients from microscopic magnetic probes and high quality factors makes detection of a single electron spin resonance theoretically possible. Because spatial resolution is limited by the ability to detect the signal from a the volume element to be imaged this high sensitivity holds the key to obtaining extremely high spatial resolution.

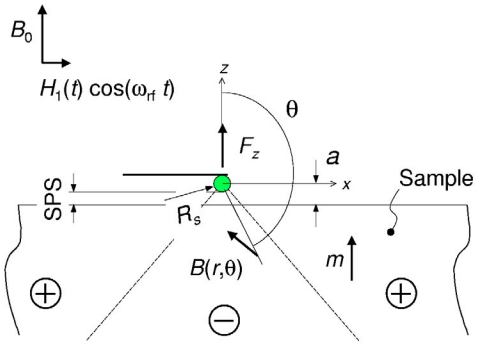

FIG. 2. Schematic diagram of the geometry of an MRFM. The micromagnet on the mechanical resonator produces an extremely inhomogeneous magnetic field that serves two purposes: (i) It couples the mechanical resonator to the magnetic moments in the sample, and (ii) it defines the spatial regions of the sample where the magnetic resonance condition is met. Magnetic resonance techniques can be employed to manipulate the magnetization $\boldsymbol{m}$ thus generating a force on the mechanical resonator at its resonance frequency that will drive it into oscillation.

The general concept of the method allows two major MRFM architectures. One places the sample on the mechanical resonator which is then coupled to an external probe magnet. This approach allows use of a relatively large probe magnet with well known magnetic properties. However the requirement that samples be placed on the resonator severely limits the applicability and usefulness of microscope based on this design. The approach we are currently pursuing in our research involves a micromagnetic probe mounted directly on the mechanical resonator brought in the close vicinity of the sample. This will allow true scanning operation on a sample of arbitrary size, however the fabrication of a micromagnet with well known magnetic properties is more challenging. For this reason accurate mapping of the magnetic field of a probe micromagnet is very important for the development of the MRFM.

Scanning mode magnetic resonance force microscopy has several significant advantages over conventional scanning probe techniques. These techniques usually provide information limited to the surface of a sample and cannot unequivocally identify chemical elements on this surface. On the contrary, the nonuniform magnetic field of the probe magnet gives the MRFM a unique ability to select a subsurface slice of a sample for study; it is only in this region defined by the externally applied *rf* field, that the magnetic resonance condition is satisfied. Moreover, magnetic resonance delivers material specific information thus

enabling MRFM to study chemical content of various substances. All these features make the MRFM a potentially extremely powerful subsurface characterization tool which can find a wide application in various fields of science and technology.

Reliable interpretation of MRFM signals is requires thorough and detailed understanding of the interaction between the micromagnetic probe and the sample. Here we address this problem is some detail.

IV. THEORETICAL ANALYSIS

In order to perform both analytical and numerical analysis we introduce a geometrical model representing a typical scanning MRFM geometry (Fig. 2). The probe magnet, mounted on a mechanical resonator with resonant frequency $f_c = \omega_c/2\pi$, is modeled as a sphere of a radius R_S uniformly magnetized along the direction of the external magnetic field $\boldsymbol{B}_0$. The sample magnetization $\boldsymbol{m} = \{0, 0, m_z\}$ is assumed to be uniform throughout the volume of the sample. The in-plane components of magnetization are ignored because they presses at frequency $\omega_L \gg \omega_c$. The resonator can oscillate only along $\hat{z}$ direction, therefore the important component of the total force of probe-sample interaction is given by

$$F_z = -\boldsymbol{e}_z \cdot \int d^3x\, [\boldsymbol{m}(\boldsymbol{x}) \cdot \boldsymbol{\nabla}] \boldsymbol{B}_{\rm tot}(\boldsymbol{x}), \qquad (2)$$

where $\boldsymbol{B}_{\rm tot}(\boldsymbol{x}) = \boldsymbol{B}_{\rm probe}(\boldsymbol{x}) + \boldsymbol{B}_0$. To further simplify calculations the high-field approximation $|\boldsymbol{B}_0| \gg |\boldsymbol{B}_{\rm probe}(\boldsymbol{x})|$ is used, hence $\boldsymbol{B}_{\rm tot}(\boldsymbol{r}) \| \boldsymbol{e}_z$.

Various rf-modulation techniques are used to manipulate the magnetic moments in the sample to create an alternating force on the mechanical magnetic resonance detector. The simplest modulation method is amplitude modulation (AM) of the *rf* power at the resonant frequency of the mechanical resonator. To simplify the evaluation of the change in magnetization of the sample under the influence of *rf* radiation we assume that the spin-lattice relaxation time T_1 of the sample material is much shorter than the oscillation period of the mechanical resonator. Under this assumption the spins in the sample are always in dynamical equilibrium.

Amplitude modulation generates a time dependent magnetization of the sample with a strong Fourier component at the resonance frequency of the mechanical resonator with an amplitude given by

$$F_z^{f_c} = -\boldsymbol{e}_z \cdot \int d^3x\, [\boldsymbol{\delta m}(\boldsymbol{x}) \cdot \boldsymbol{\nabla}] \boldsymbol{B}_{\rm tot}(\boldsymbol{x}), \qquad (3)$$

where $\boldsymbol{\delta m}(\boldsymbol{x})$ is the local change of sample magnetization during a single cycle of *rf* - modulation.

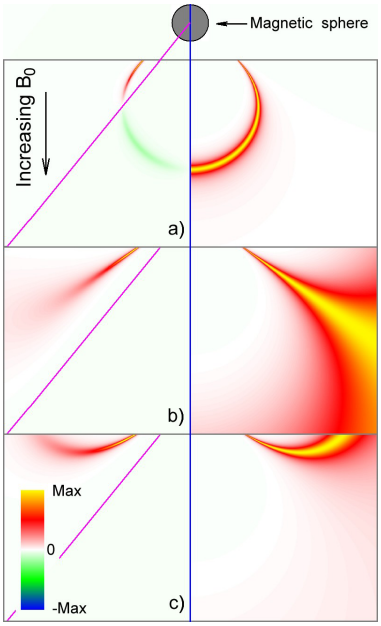

FIG. 3. Calculation of the sensitive slice shape (right hand panels) and the force slice (left hand panels) for different values of the external field B_0. For all panels $\omega_{\rm rf}/\gamma = 10000$ Gauss. The force slice is weighted by the volume element. The purple line on the left (force slices) marks the angle at which the local force changes sign (see also Fig. 2). a) ($B_0 = 9985$ Gauss) show typical sensitive slices as shells of constant field for $\gamma B_0 < \omega_{\rm rf}$. b) shows the situation for $\gamma B_0 = \omega_{\rm rf}$. Since the gradient is very small in the regions where the resonance condition is met the ratio of the line width to the gradient is very large, hence a large volume of sample meets the resonance condition. The conventional concept of a typical length scale set by the width $x_{\rm sl}$ of the sensitive slice ($x_{\rm sl} \approx \delta B_{\rm linewidth}/\nabla B$) breaks down in this case. c) $\gamma B_0 > \omega_{\rm rf}$ ($B_0 = 10005$ Gauss). Here the shape of the sensitive slice is approximately toroidal.

Analytical integration of Eq. 3 for a general experimental MRFM geometry is quite complicated, however we have done this for a few symmetric limiting cases, and these prove to be valuable guides for understanding this interaction [16]. However, due to the limiting nature of these analytical solutions, quantitative comparisons with experiment can be achieved only by numerical integration of Eq. 3. The main advantage of this approach is that the analysis of an arbitrary probe sample geometry is possible, and more realistic models of the probe micromagnet can be implemented. The detailed description of both analytical and numerical approaches is given in [16].

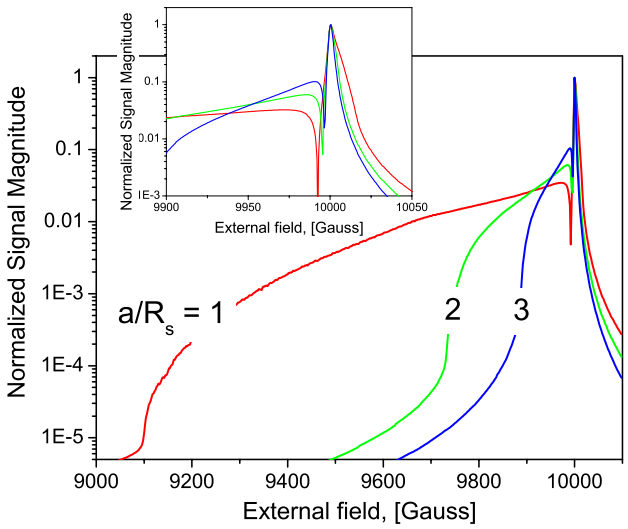

FIG. 4. Numerically calculated MRFM signal vs. external magnetic field calculated for various sample-probe separations a measured in units of the radius of the probe magnet R_S. This calculation was performed for a semi-infinite bulk sample assuming that the resonant field in the absence of the probe magnet is 10000 Gauss. The inset shows an expanded view of the main peak of the resonance.

The result of the numerical analysis of the probe sample interaction is presented in Fig. 3. This shows the evolution of the sensitive slice and of the force slice under typical experimental conditions that include continuous sweep of the external magnetic field B_0 as the frequency of the *rf* field $\omega_{\rm rf}$ is kept constant. The term "sensitive slice" refers to the sample volume in which magnetic moments interact resonantly with the *rf* field: that is, the region where $\omega_{\rm rf} = \gamma B_{tot}(\boldsymbol{x})$ is satisfied. The right hand panel of Fig. 3 shows the change in the sample spin magnetization due to suppression by the *rf* field as a function of spatial position within the sample. The concept of the force slice describes coupling of the magnetic moments in the sample to the probe magnet on the mechanical resonator. This is the volume of the sample that actually contributes to the alternating force driving the mechanical resonator, that is, it is the volume where the integrand of Eq. 3 is nonzero. The left hand panel of Fig. 3 shows the local force contribution as a function of spatial position within the sample. Note that the sign of the local force contribution is defined by the sign of the appropriate component of the gradient of magnetic field of the probe. Due to the dipolar nature of the probe magnetic field this sign depends on the position of the point of interest relative to the probe magnet. The line on the left hand panel of Fig. 3 shows where this gradient turns passes through zero and changes sign. Clearly, force contributions from different parts of the sample can have opposite signs Fig. 3a thus cancelling each other.

The model developed in Ref. [16] allows us to predict the evolution of the MRFM signal as experimental parameters are changed. Fig. 4 shows the MRFM signal calculated for various probe sample separations. It can be seen that, independent of the magnitude of the probe-sample separation, each curve exhibits a strong peak near the resonant field. However the leading edge of the signal shifts to lower values of external magnetic field as the probe is brought closer to the surface of the sample. The offset of the leading edge of the signal relative to the main peak is equal to the magnitude of the probe magnetic field at the surface of the sample directly below the probe; this field increases as the probe-sample separation is decreased.

The main peak of the sample corresponds to the condition when the majority of the sample is resonant and the concept of a well defined sensitive slice has broken down Fig. 3c. The region of interest for the MRFM operating as a high spatial resolution subsurface imaging tool is near the leading edge of the signal where the sensitive slice is well defined and the number of spins contributing to the signal, and thus the signal itself, is small.

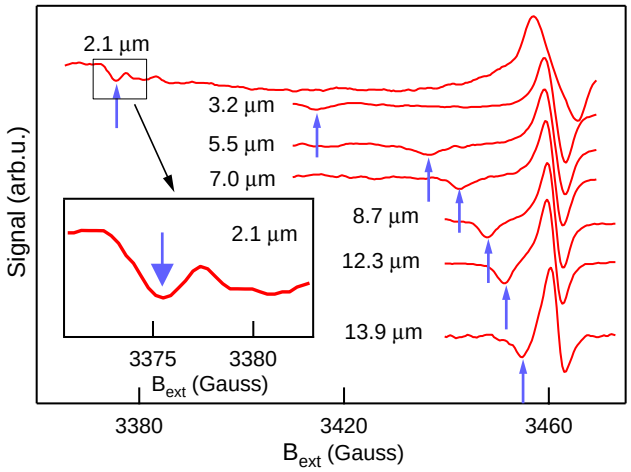

FIG. 5. The electron spin resonance signal from a 100 nm DPPH film at various probe-sample separations detected using frequency modulation of the *rf* field at $T = 4$ K. Arrows mark the position of the peak corresponding to the leading edge of the signal. The inset shows the leading edge signal detected at 2.1 μm probe-sample separation. It can be seen that the signal-to-noise ratio is not limited by the thermo-mechanical noise of the mechanical resonator.

V. EXPERIMENTAL RESULTS

We have experimentally studied the evolution of the leading edge of MRFM signal. For this the Electron Spin Resonance (ESR) signal from a 100 nm thick DPPH film was used. Because amplitude modulation of the applied microwave radiation creates undesirable excitation of the mechanical resonator complicating detection of weak signals we chose to perform our experiments using frequency modulation (FM). The power of the *rf* radiation was kept constant as its frequency was modulated at f_c. This reduces the coupling of *rf* field to the resonator, however FM changes the shape of MRFM signal; instead a derivative of the AM signal is detected. In this case the leading edge of the signal appears as a peak that shifts its position as the probe is moved toward the sample.

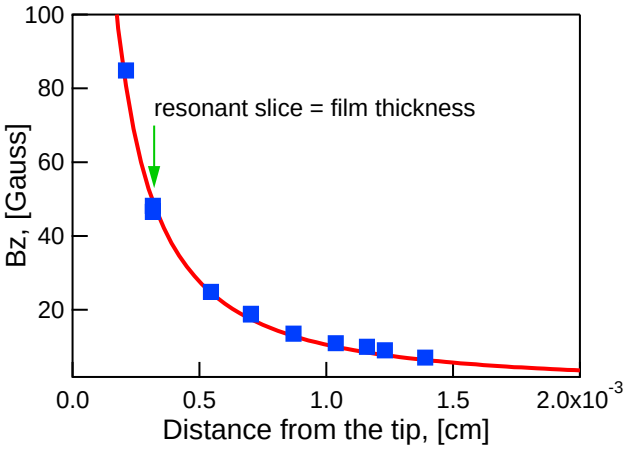

FIG. 6. Magnetic field of the probe magnet vs. the distance from its tip. The solid curve presents the result of the micromagnetic simulations of the expected magnetic field of the probe magnet used in the experiment. The solid squares are experimentally measured values of the field of the probe magnet.

Fig. 5 shows several MRFM signals recorded at various probe-sample separations and demonstrates the behavior predicted by the model. All the curves exhibit a large probe position independent signal at the resonant field (where the probe field is zero) and a much smaller leading edge feature corresponding the sensitive slice entering the sample. The latter shifts to lower values of the external magnetic field as the probe approaches the sample surface. As it has been mentioned above, the relative position of this feature is a direct measure of the magnetic field of the probe magnet at the sample surface;this feature provides a means of experimentally measuring the probe field. The filled squares in Fig. 6 show the decrease of the field of the probe magnet with increasing separation from the probe. The solid curve presents the results of micromagnetic simulations of magnetic field of a micromagnet with the same parameters as those of the probe magnet used in the experiment. The experimental data is in excellent agreement with the theoretical curve.

Precise understanding of the field of a particular probe magnet enables us, using the model of probe-sample interaction described above, to predict the shape of the sensitive slice for a scanning probe-sample geometry. This ability is extremely important for development of a subsurface 3D MRFM imaging technique similar to conventional Magnetic Resonance Imaging (MRI). In practice this method will be based on a data processing technique which extracts 3D image from a collection of intersecting subsurface sensitive slices obtained at various spatial probe positions and values of external magnetic field. Precise knowledge of the field profile of the probe magnet will be crucial input for such a technique.

Knowledge of the of the field of the probe magnet has also enabled us to estimate the number of spins contributing to the measured signal at various values of external magnetic field and probe sample separation. The leading edge feature observed at a probe-sample separation of 2.1 μm corresponds to a signal from approximately 10^4 fully polarized electron spins. As can be seen in the inset to Fig. 5 the force sensitivity of our apparatus is not yet limited by the thermo-mechanical noise of the cantilever, which is estimated to set our detection limit at approximately 10^3 fully polarized electron spins. Therefore, improvements in noise-rejection techniques are expected to improve the sensitivity of our microscope by an order of magnitude in the near future.

VI. IMAGE DECONVOLUTION

The detailed understanding of the probe-sample interaction described in the previous sections enables us to proceed toward the development of special imaging techniques that will unable subsurface imaging of single electron qubits with MRFM. The pioneering steps in this direction were made by O. Züger and D. Rugar who successfully demonstrated mapping of the sensitive slice from a large magnet using ESR measurements on a sample much smaller than the gradient magnet [17]. Subsequently, O. Züger, *et al.*, demon-

strated MRFM imaging of the nuclear spin density in a $\sim 10\mu$m irregularly-shaped particle [18].

However, as our analysis of probe-sample interaction shows, any attempt at subsurface inhomogeneous spin density imaging in sample with characteristic dimensions much larger than those of the probe magnet will be complicated by the position dependence of the probe-sample interaction forces originating from the dipolar nature of the magnetic field of the probe magnet. The situation will be complicated even further by the presence of two or more spin species with relatively close but still different gyromagnetic ratios, which means there will be several sensitive slices in the sample. It is clear that the detailed analysis of image deconvolution from MRFM data has yet to be done. In this section we will outline our directions for developing subsurface single spin imaging for quantum computing.

In general, the problem of extraction of the spin density profile from the signal measured by a cantilever is related to the image deconvolution problems encountered in MRI and digital image processing. As such, it can be addressed using the similar techniques and algorithms.

In the most general case, the AC signal, $F(\mathbf{r})$, measured by the cantilever, which can be the amplitude, frequency or phase shift of the mechanical oscillation, is given by the integral over the spin density, $m(\mathbf{r}')$,

$$F(\mathbf{r}) = \int f(\mathbf{r}, \mathbf{r}')m(\mathbf{r}')d\mathbf{r}'. \tag{4}$$

Here, the kernel $f(\mathbf{r}, \mathbf{r}')$ is related to the specific form of the magnetic field gradient generated by the tip, the form of the sensitive slice, effects of the sample boundaries on the cantilever (e.g., modification of the Q-factor), external magnetic and *rf*/microwave field inhomogeneities. Such a form for the signal implies that the scanning over real space $\mathbf{r}$ is performed while keeping the external experimental parameters, external magnetic field and *rf* or microwave frequency constant. Depending on a particular technique, the vector nature of the magnetization $m(\mathbf{r})$ can be either unimportant (if the probe tip field is weaker than the external field), or important (zero external field). The two cases are conceptually similar and hence we will focus here on the scalar case.

Eq. 4 is the Fredholm integral equation of the first kind, which is notoriously ill-conditioned. Even small error in the measurement of the cantilever response $F(\mathbf{r})$ can cause a large change in the deduced spin density $m(\mathbf{r})$. This is easy to understand since integration is a smoothing operation and any integrable local singularity in m can cause only a small change in F. To tackle such problems, one has to make assumptions about the properties of the function m. Formally, this is achieved by filtering or regularization techniques. The most common implicit assumption is that the function $m(\mathbf{r})$ be smooth. This is a valid approximation if only coarse-grained polarization densities are of interest, however, hardly adequate for the single spin detection case. As a practical issue, the highest achievable spatial resolution under any circumstances is given by the spatial resolution of the scanning probe, however, measurement noise may further reduce it. Probing the polarization distribution with single spin resolution is therefore a hard problem since the individual spin distribution is inherently point-like. Moreover, it is not the sensitive slice that is imaging the spin distribution, but rather individual spins imaging the sensitive slice.

There are two main techniques that can be applied to deduce the spin density from the measured signal, which should be applicable both in the smooth and the single-spin cases. These are: (a) Fourier transform-based deconvolution with filtering, and (b) regularized numerical solution of Eq. (4). The deconvolution technique is relatively fast, but is only applicable for homogeneous kernels, $f(\mathbf{r}, \mathbf{r}') = f(\mathbf{r} - \mathbf{r}')$, which is the case when the spurious effects of sample boundaries and other inhomogeneities are either negligible, or can be removed. The direct solution technique is more general, but computationally intensive and also requires assumptions about the properties of the solution.

A. Fourier deconvolution

In the special case when the kernel of Eq. 4 is homogeneous,

$$F(\mathbf{r}) = \int f(\mathbf{r} - \mathbf{r}')m(\mathbf{r}')d\mathbf{r}', \tag{5}$$

the magnetic polarization $m(r)$ can be obtained using the Fourier deconvolution technique. Formally,

$$\tilde{m}(\mathbf{k}) = \frac{\tilde{F}(\mathbf{k})}{\tilde{f}(\mathbf{k})}, \tag{6}$$

$$m(\mathbf{r}) = \int e^{i\mathbf{kr}}\tilde{m}(\mathbf{k}). \tag{7}$$

In reality however, directly applying the deconvolution technique to the noisy data F is likely to amplify the noise in m, particularly at short wave lengths, since the instrument function $\tilde{f}$ vanishes for large enough $\mathbf{k}$

(greater than the inverse width of the sensitive slice). To avoid this problem, heuristically, one may introduce the cutoff in the denominator, that will effectively suppress the short-wave length noise, but also at the same time limit the spatial resolution [18]:

$$\tilde{m}(\mathbf{k}) = \frac{\tilde{F}(\mathbf{k})\tilde{f}^*(\mathbf{k})}{|\tilde{f}(\mathbf{k})|^2 + C}, \tag{8}$$

where $\tilde{f}^*$ is the complex conjugate of $\tilde{f}$, and C is a positive constant that is related to the noise.

Alternatively, the optimal (Wiener) filter [19] can be applied,

$$\tilde{m}(\mathbf{k}) = \frac{\tilde{F}(\mathbf{k})}{\tilde{f}(\mathbf{k})}\left(1 - \frac{|N(\mathbf{k})|^2}{|F(\mathbf{k})|^2}\right). \tag{9}$$

The Wiener filter implies knowledge of the measurement noise power spectrum, $|N(\mathbf{k})|^2$, the noise in the measurement of $F(\mathbf{r})$. It is optimal in the sense of the $m(\mathbf{r})$ error-squared integrated over the volume of the sample. The main challenge in applying the optimal filter is in determining the noise spectrum. We will approach this problem by fitting and modeling the experimentally measured spectrum of $F(\mathbf{r})$.

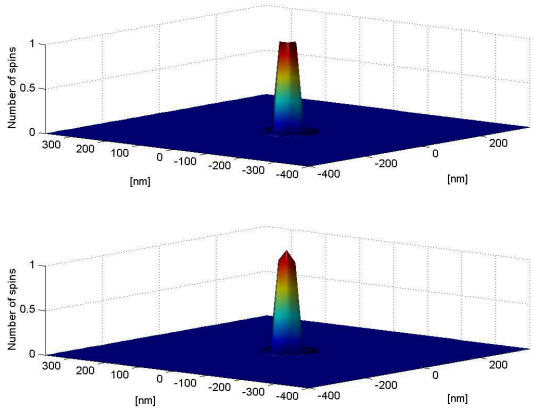

FIG. 7. An example of numerical image deconvolution using a 3D Fast Fourier Transform. a) A 2D slice through the 3D spin distribution pattern input into the numerical experiment. b)A 2D slice through the recovered 3D image of the original spin distribution.

Computationally, the deconvolution technique is best implemented using the multidimensional Fast Fourier Transforms (FFT). Fig. 7 demonstrates application of the 3D FFT to a set of data obtained from numerical simulation of interaction of spherical MRFM probe magnet with a point 3D spin distribution buried in a zero spin substance. The geometry of the simulation has been described earlier in the paper. It can be seen in Fig. 7b, that the recovered image of the spin distribution is in good agreement with the original data.

B. Discretized solution of the signal Integral equation

In some cases, the homogeneity approximation needed to apply the Fourier deconvolution techniques is not valid, for instance when the translational symmetry of the kernel f is broken due to the surface effects or inhomogeneity of the external magnetic field or *rf*/microwave radiation. In this case, the kernel cannot be reduced to the homogeneous form, and other numerical techniques for the solution of the integral Eq. 4 have to be applied.

Assume that the MRFM signal has been measured on a 3D grid, F_i, and the signal is related to the magnetization on the same or some other related grid, m_i. To find the magnetization one needs to solve the system of linear equations,

$$\sum_j f_{ij} m_j = F_i, \tag{10}$$

which is simply a discretized form of the original integral Eq. 4. While it is relatively straightforward to solve such a system of equations for matrix dimensions up to a few thousand, the problem is that the matrix f_{ij} is likely to be ill-conditioned and hence the solution may have little if anything to do with the actual spin distribution. To rectify this problem, various regularization techniques are often used. All of them rely on procedures for minimization of a functional that can be tuned to incorporate the expected properties of the actual underlying function $m(\mathbf{r})$, such as smoothness, stability, or likelihood. An example of such functional that favors smooth functions is

$$\sum_i (F_i - \sum_j f_{ij} m_j)^2 + \lambda \sum_{i,j} H_{ij} m_i m_j, \tag{11}$$

where H_{ij} is a positive semidefinite matrix that has a zero eigenvalue that corresponds to constant m_i [19]. By tuning the parameter λ, from 0 to infinity, one can manage the trade-off between the agreement with the measured data and the expected behavior of the unknown function. Similarly, functionals can be constructed that reflect essentially any *a priori* knowledge of the spin distribution.

While computationally significantly more intensive than the fast-Fourier transform deconvolution techniques described in the previous subsection, the direct regularized method represents a viable alternative for the experimental situations when the extraneous effects make the application of the FFT-based methods impossible. Where possible, the two described methods can be used for cross-check purposes.

VII. CONCLUSIONS

We have experimentally verified the validity of our model describing the probe sample interaction in Magnetic Resonance Force Microscopy. This enables us to characterize the sensitivity of our scanning probe MRFM and provides the basis for development of data deconvolution that will enable 3D subsurface imaging of single electron qubits of a silicon-based quantum computer using the MRFM.

ACKNOWLEDGMENTS

We gratefully acknowledge the important contributions of our collaborators M. L. Roukes and R. G. Clark. This work was supported by ARDA and the US DOE.

---

* present address: Laboratory for Muon-Spin Spectroscopy (LMU), Paul Scherrer Institute, CH-5232 Villigen PSI, Switzerland.

[1] N. Gershenfeld and I. Chuang, Scientific American **278**, 66 (1998).
[2] P. Shor, in *Proceedings of the 35th Annual Symposium on the Foundations of Computer Science* (IEEE, Los Alamitos, CA, 1994), p. 124.
[3] P. Shor, Siam Journal On Computing **26**, 1484 (1997).
[4] G. Ortiz, J. E. Gubernatis, E. Knill, and R. Laflamme, Phys. Rev. A **6402**, 2319 (2001).
[5] R. Hughes *et al.*, Physical Review Letters **77**, 3240 (1996).
[6] C. Sackett *et al.*, Nature **404**, 256 (2000).
[7] B. E. Kane, Nature **393**, 133 (1998).
[8] R. Vrijen *et al.*, Physical Review A **6201**, 2306 (2000).
[9] G. Navon *et al.*, Science **271**, 1848 (1996).
[10] R. Tycko *et al.*, Science **268**, 1460 (1995).
[11] J. M. Kikkawa and D. D. Awschalom, Science **287**, 473 (2000).
[12] Y. S. Greenberg, Rev. Mod. Phys. **70**, 175 (1998).
[13] J. A. Sidles, Appl. Phys. Lett. **58**, 2854 (1991).
[14] J. A. Sidles *et al.*, Rev. Mod. Phys. **67**, 249 (1995).
[15] P. C. Hammel, Z. Zhang, G. J. Moore, and M. L. Roukes, J. Low Temp. Phys. **101**, 59 (1995).
[16] A. Suter, D. V. Pelekhov, M. L. Roukes, and P. C. Hammel, *Probe-Sample Coupling in the Magnetic Resonance Force Microscope*, J. Magn. Reson., in press, 2002.
[17] O. Züger and D. Rugar, Appl. Phys. Lett. **63**, 2496 (1993).
[18] O. Züger, S. T. Hoen, C. S. Yannoni, and D. Rugar, J. Appl. Phys. **79**, 1881 (1996).
[19] W. H. Press *et al.*, *Numerical Recipes in C*, 2nd ed. (Cambridge Univ. Press, Cambridge, 1997).